

Master's Thesis

석사 학위논문

Characterization of Surface Free Energy of Cathode Materials for Lithium-ion Batteries

Junmin Lee(이 준 민 李 峻 珉)

Department of Energy Systems Engineering

에너지시스템공학전공

DGIST

2013

Master's Thesis

석사 학위논문

Characterization of Surface Free Energy of Cathode Materials for Lithium-ion Batteries

Junmin Lee(이 준 민 李 峻 珉)

Department of Energy Systems Engineering

에너지시스템공학전공

DGIST

2013

Characterization of Surface Free Energy of Cathode Materials for Lithium-ion Batteries

Advisor : Professor Hochun Lee

Co-advisor : Doctor Su-An Choi

by

Junmin Lee

Department of Energy Systems Engineering

DGIST

A thesis submitted to the faculty of DGIST in partial fulfillment of the requirements for the degree of Master of Science in the Department of Energy Systems Engineering. The study was conducted in accordance with Code of Research Ethics¹.

07. 09. 2013

Approved by

Professor Hochun Lee

(Advisor)

Doctor Su-An Choi

(Co-Advisor)

¹ Declaration of Ethical Conduct in Research: I, as a graduate student of DGIST, hereby declare that I have not committed any acts that may damage the credibility of my research. These include, but are not limited to: falsification, thesis written by someone else, distortion of research findings or plagiarism. I affirm that my thesis contains honest conclusions based on my own careful research under the guidance of my thesis advisor.

Characterization of Surface Free Energy of Cathode Materials for Lithium-ion Batteries

Junmin Lee

Accepted in partial fulfillment of the requirements for the degree of
Master of Science.

07. 09. 2013

Head of Committee Hochun Lee (인)

Prof. 이호춘

Committee Member Su-An Choi (인)

Dr. 최수안

Committee Member Seung-tae Hong (인)

Prof. 흥승태

MS/ES 이 준 민 . Junmin Lee. Characterization of Surface Free Energy of Cathode
201124015 Materials for Lithium-ion Batteries. Department of Energy Systems
Engineering. 2013. P. Advisor Prof. Hochun Lee, and Co-Advisor Dr. Su-An
Choi.

Abstract

While the lithium-ion batteries (LIBs) are expanding their application area from mobile IT devices to the large scale power sources for electric vehicles and renewable energy storages, the limited cycle life of the present LIBs has been pointed out as the main obstacle. The degradation of LIBs employing LiMn_2O_4 and LiCoO_2 cathode materials is known to be initiated by the metal dissolution from the cathode materials. Owing to the slow kinetics of the metal dissolution behavior, the quantitative analysis of the trace amounts of dissolved metal ions has been relied on the spectroscopic techniques such as the inductive coupled plasma (ICP) or the atomic adsorption spectroscopy (AAS). These conventional methods take at least several days and fail to provide any information on the cathode surface properties. We herein report that the SFE of cathode materials is closely related to their metal dissolution behavior. The SFEs of various types of LiCoO_2 and LiMn_2O_4 are obtained by the contact angle measurement: the liquid adsorption method for powder samples and the sessile drop method for electrode samples. We confirm that the metal dissolution is determined dominantly by the polar component of the SFE of the cathode surface. We also found that the Al_2O_3 coating suppresses the metal dissolution, which is ascribed to the deceased polarity of cathode surface. The basic polarity of cathode electrodes is smaller than that of powders, which suggests a possibility that the metal dissolution can be suppressed through the optimization of the composite electrode components (binders and conductive carbons). We also confirmed the correlation of the SFEs with the types of crystal structures, which was examined by using SEM and XRD analysis.

Keywords: Lithium-ion batteries, LiMn_2O_4 , LiCoO_2 , Metal dissolution, Surface free energy, Polarity

Contents

Abstract	i
List of contents	iii
List of figures	v
List of tables	viii
1. Introduction	1
1.1 Overview	1
1.2 Theory of surface free energy calculation by contact angle measurement	2
1.3 Capillary rising method for porous materials	8
1.4 Dissolution mechanism of cathode materials for Li-ion batteries ·	10
1.5 Influence of cathode crystal structure to metal dissolution	11
1.6 Examples of surface free energy usages to analyze the characteristics of Li-ion batteries	12
2. Experimental	13
2.1 Sessil drop method	13
2.2 Adsorption method	15
2.3 Measurement of metal dissolution	18
3. Results and discussion	19
3.1. Correlation of the surface free energies of LiMn_2O_4 powder with Mn dissolution	19
3.2 Correlation of the surface free energies of LiMn_2O_4 electrode with Mn dissolution	21
3.3 Analysis the crystal structures of LiMn_2O_4	23
3.4 Correlation of the surface free energies of LiMn_2O_4 by increasing Al_2O_3 coating amount with Mn dissolution	26
3.5 Acid and base part separation of polar surface free energy	

of LiMn_2O_4	28
3.6 Correlation of the surface free energies of LiCoO_2 powder with Co dissolution	30
3.7 Correlation of the surface free energies of LiCoO_2 electrode with Co dissolution	32
3.8 Correlation of the surface free energies of LiCoO_2 by increasing Al_2O_3 coating amount with Co dissolution	33
3.9 Acid and base part separation of polar surface free energy of LiCoO_2	35
4. Conclusions	36
References	37
Summary (국문요약)	38

Acknowledgement (감사의 글)

Curriculum Vitae

List of figures

Fig. 1 Schematic experimental setup for contact angle measurements at powders

Fig. 2 Schematic description of dissolution mechanisms of LiMn_2O_4

Fig. 3 Figure from Hirayama, Ido. Schematics of surface reactions for (111) and (110) crystal planes of LiMn_2O_4 characterized by in situ XRD and XRR measurements and ex situ TEM observations

Fig. 4 Schematics of SFEs factors between solid, liquid and vapor

Fig. 5 DI water drop on LiCoO_2 Surface

Fig. 6 Fiber chamber SH0620 (Krüss, Hamburg, Germany)

Fig. 7 Formamide adsorption mass change by time of LiCoO_2 powder

Fig. 8 Adsorped mass of probe liquids to filter

Fig. 9 Co Dissolution of LiCoO_2 with (a) Electrode in Large Bottle with Shaker (30rpm), (b) Electrode in Small bottle and (c) Same amount of powder of Electrode in Small Bottle

Fig. 10 Correlation of Mn dissolution with (a) Total SFEs (b) polarity (c) dispersity of LiMn_2O_4 powder

Fig. 11 Correlations of Mn dissolutions with (a) Total SFEs, (b) polarity and (c) dispersity of LiMn_2O_4 electrodes

Fig.12 SEM images of LiMn_2O_4 powders. (a) Mitsui, (b) Nikki, (c) LNF_1, (d) LNF_2

Fig. 13 XRD Patterns of LiMn_2O_4 powders (a) Mitsui, (b) Nikki, (c) LNF_1, (d) LNF_2

Fig. 14 Correlations of SFEs and Mn dissolution of LiMn_2O_4 powders by increasing Al_2O_3 coating amount with (a) Total SFEs, (b) polarity and (c) dispersity

Fig. 15 SEM images of LiMn_2O_4 powders by increasing Al_2O_3 coating amount. Al was coated (a) much (b) medium (c) less on the LiMn_2O_4 surface.

Fig. 16 Acid and base components of LiMn_2O_4 (a) powders and (b) electrodes by

calculation from diiodomethane, formamide and water contact angles

Fig. 17 Mn Dissolutions of LiMn_2O_4 (a) powders and (b) electrodes normalized by BET

Fig. 18 Correlations of Co dissolutions with (a) Total SFEs, (b) polarity and (c) dispersity of LiCoO_2 Powders

Fig. 19 Correlations of Co dissolutions with (a) Total SFEs, (b) polarity and (c) dispersity of LiCoO_2 Electrodes

Fig. 20 Correlations of SFEs and Co dissolutions of LiCoO_2 powders by increasing Al_2O_3 coating amount with (a) Total SFEs (b) Polarity (c) Dispersity

Fig. 21 Acid and base components of LiCoO_2 (a) powders and (b) electrodes by calculation from diiodomethane, formamide and water contact angles

Fig. 22 Co Dissolutions of LiCoO_2 (a) powders and (b) electrodes normalized by BET

List of tables

Table 1: Critical surface tensions of polymeric solids

Table 2: N/Metal and S/Metal ratios measured by XPS after adsorption of NH₃ or SO₂ at 80°C on LiCo_{1-x}Al_xO₂ Samples (0 ≤ x ≤ 0.50), compared with various oxides in the same experimental conditions

Table 3: SFE properties of probe liquids

Table 4: Correlations of surface free energies of LiMn₂O₄ powder with Mn dissolutions

Table 5: Correlations of surface free energies of LiMn₂O₄ electrodes with Mn dissolutions

Table 6: Correlations of surface free energies of LiMn₂O₄ powder by increasing Al₂O₃ coating amount with Mn dissolutions

Table 7: Correlations of surface free energies of LiCoO₂ powder by increasing Al₂O₃ coating amount with Co dissolutions

1. Introduction

1.1 Overview

LiMn_2O_4 is one of promising candidates for electrical vehicles for high power with long cycle life. But degradation of cycle life is one of serious problem of LiMn_2O_4 . Main cause of cycle life degradation is metal dissolution of cathode. So this study mainly focused on to characterize the surface free energies (SFEs) of LiMn_2O_4 and LiCoO_2 for LIBs to predict metal dissolution behaviors to improve the capacity degradation.

Contact angles were measured to calculate SFEs of cathodes. Contact angles are measured by the liquid adsorption method for powder samples or by the sessile drop method for electrode samples. Sessil drop method was much easier than adsorption method: the contact angles of electrodes were measured directly by dropping probe liquids on electrode surfaces. But the contact angles of cathode powders were calculated from mass changes of cathode powders from adsorbing probe liquids by time. So there were many noises involved, such as powder loading to fiber chamber, capillary constant calculation, the humidity of a room and temperature change. But the SFEs of cathode electrodes were calculated from the mixture of cathode powder, conductive carbon and binder. So to characterize the real characteristic cathode powders should be measured. Metal dissolution measurements were done by atomic adsorption spectroscopy (AAS) (Shimazu AA7000) to confirm the correlation with SFEs.

1.2 Theory of Surface Free Energy Calculation by Contact Angle Measurements

The analysis of interaction between liquid and solid by contact angle measurement has begun from early 18th century by Thomas Young[1]. Base of these studies, the calculation method of SFE was suggested by D. K. OWENS in 1969[2]. He measured surface energy of solids and resolved the surface energy into dispersion and dipole-hydrogen bonding forces by based on measuring contact angles with water and methylene iodide. Measured surface energies were well matched with Zisman's γ_c (Critical Surface Tension: Total surface energy) [3] and Fowkes' γ_d (Dispersion Force)[4].

Polymeric Solid	γ_c
Polymethacrylic ester of Φ' -octanol ^a	10.6
Polyhexafluoropropylene	16.2
Polytetrafluoroethylene	18.5
Polytrifluoroethylene	22
Polyvinylidene fluoride	25
Polyvinyl fluoride	28
Polyethylene	31
Polytrifluorochloroethylene	31
Polystyrene	33
Polyvinyl alcohol	37
Polymethyl methacrylate	39
Polyvinyl chloride	40
Polyvinylidene chloride	40
Polyethylene terephthalate	43
Polyhexamethylene adipamide	46

Table 1. Critical surface tensions of polymeric solids [3]

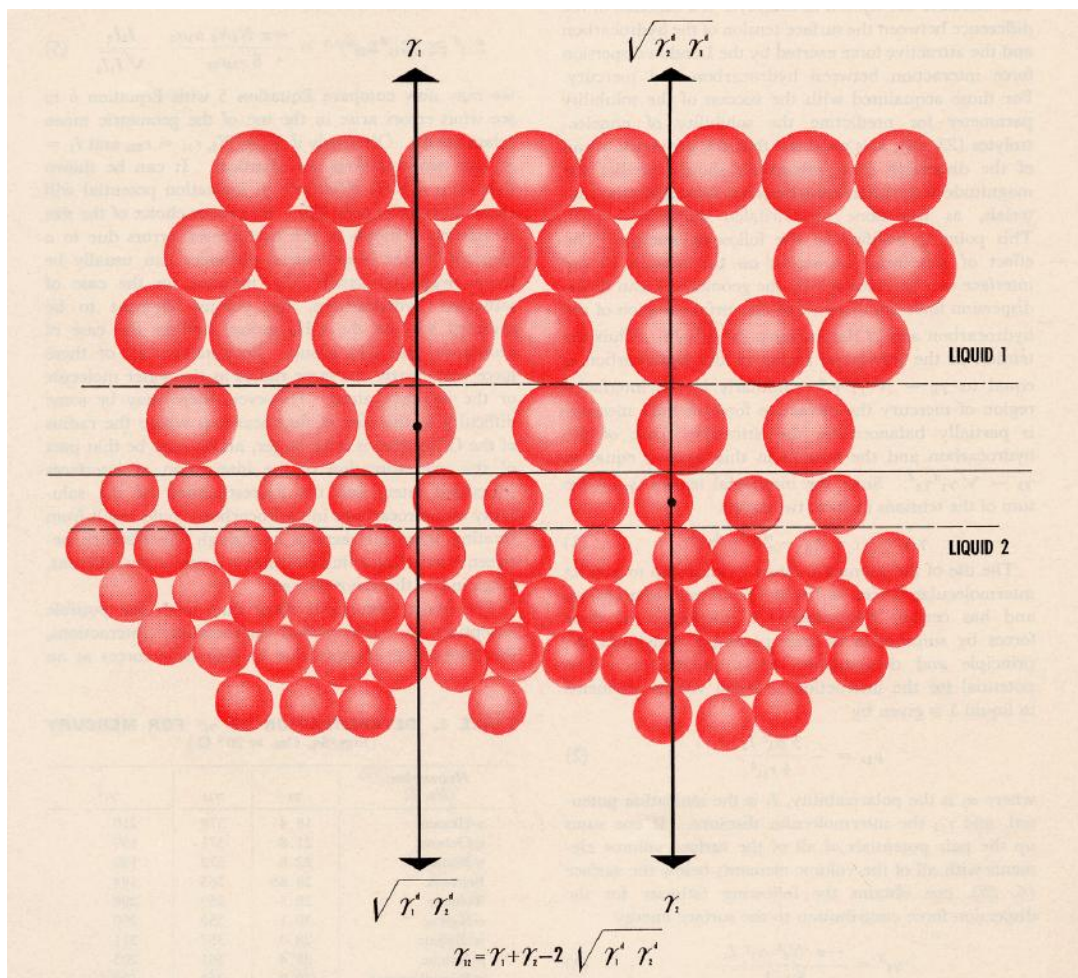


Fig. 1. A very simple Fowkes' model of interface [4]

At the interface between mercury and a saturated hydrocarbon the molecules in the two “interfacial region” are subject to the resultant force field made up of components arising from bulk attractive forces in each phase, and the London dispersion forces operating across the interface itself [4].

In 1987 C.J. van Oss, M.K. Chaudhury and R.J. Good (vOCCG) [5] separated polarity of monopolar surface into acid and base part of SFE. In 1993 Bronislaw Jańczuk summarized the components of the surface tension of some liquids from interfacial liquid-liquid tension

measurements [6]. In summarization of Bronislaw Jańczuk study, the liquid surface tension or solid SFE can be expressed as the sum of the parts of different kind of intermolecular interactions [7].

$$\gamma = \gamma^d + \gamma^i + \gamma^p + \gamma^h + \gamma^\pi + \gamma^{ad} + \gamma^e \quad (\text{Eq. 1.1})$$

where γ is the surface tension of a liquid or the solid SFE, and index d refers to dispersion, i to induced dipole-dipole, p to dipole-dipole, h to hydrogen bonding, π to π bonding, e to electrostatic, and ad to acceptor-donor interactions. Practically it can be written

$$\gamma = \gamma^d + \gamma^n \quad (\text{Eq. 1.2})$$

where γ^n is the nondispersion component of SFE of a liquid or solid surface tension. This component is sum of all parts of the surface tension resulting from the nondispersion intermolecular interactions present in a given phase.

The interfacial free energy of solid-liquid or liquid-liquid as a function of the geometric mean of dispersion and nondispersion intermolecular interaction [2, 7-9] can be expressed

$$\gamma_{12} = \gamma_1 + \gamma_2 - 2(\gamma_1^d \gamma_2^d)^{1/2} - 2(\gamma_1^n \gamma_2^n)^{1/2} \quad (\text{Eq. 1.3})$$

where 1 and 2 refer to two immiscible phases in contact with their own vapor, and the index 12 refers to two phases being in contact with each other after equilibration. γ_1^d value, γ_2^d and γ_2^n component of the liquid surface tension can be calculated from Eq 1-2

and 1-3 on the basis of interfacial tension (γ_{12}) measurements. If the liquid 1 is hydrocarbon Eq. 1-3 can be rewritten.

$$\gamma_2^d = (\gamma_1 + \gamma_2 - \gamma_{12})^2 / 4\gamma_1 \quad (\text{Eq. 1.4})$$

The dispersion and nondispersion components can be also be calculated on the basis of the Young's equation [1, 2, 7-9].

$$\gamma_L \cos \theta_L = -\gamma_L + 2(\gamma_L^d \gamma_S^d)^{1/2} + 2(\gamma_L^n \gamma_S^n)^{1/2} \quad (\text{Eq. 1.5})$$

L and S refer to liquid and solid, respectively. If γ_S^d and γ_S^n are known for a given liquid on the surface of two different solids, γ_L^d and γ_L^n can be easily calculated by Eq. 1-5. In the case when SFE of solid results only from dispersion intermolecular interactions Eq. 1-5 can be resolved into the form

$$\gamma_L^d = \gamma_L^2 (\cos \theta_L + 1)^2 / 4\gamma_S \quad (\text{Eq. 1.6})$$

vOCG [5, 10, 11] suggest that from Eq. 1-4 there can be obtained the components of the surface tension resulting from Lifshitz-van der Waals intermolecular interactions, which constitute the equation

$$\gamma^{LW} = \gamma^d + \gamma^i + \gamma^p \quad (\text{Eq. 1-7}).$$

According to vOCG [11] the SFE of solid or liquid surface tension can be expressed as the sum of two components,

$$\gamma = \gamma^{LW} + \gamma^{AB} \quad (\text{Eq. 1.8})$$

where γ^{AB} is the component resulting from Lewis acid-base intermolecular interactions. The γ^{AB} component can be expressed to the equation

$$\gamma^{AB} = 2(\gamma^+\gamma^-)^{1/2} \quad (\text{Eq. 1.9})$$

where γ^+ and γ^- are the nonadditive parts of the liquid surface tension or solid SFE resulting from electron-accepter and electron-donor interactions, respectively.

Combining Eq. 1-9 into 1-8, we have

$$\gamma = \gamma^{LW} + 2(\gamma^+\gamma^-)^{1/2} \quad (\text{Eq. 1.10})$$

Considering Eq. 1-10, vOCG [5, 10, 11] derived the equation describing the work of adhesion of phase 1 to phase 2. In the case of two liquids that are in contact this equation assume the form

$$\gamma_1 + \gamma_2 \sim \gamma_{12} = 2(\gamma_1^{LW}\gamma_2^{LW})^{1/2} + 2(\gamma^+\gamma^-)^{1/2} + 2(\gamma^-\gamma^+)^{1/2} \quad (\text{Eq. 1.11})$$

In the case when $\gamma_L = \gamma_1$ Eq. 1-11 can be rewritten in the form of

$$\gamma_2^{LW} = (\gamma_1 + \gamma_2 - \gamma_{12})^2 / 4\gamma_1 \quad (\text{Eq. 1.12})$$

According to vOCG [5, 10, 11], exists between the contact angle and components of solid SFE and liquid surface tension can be expressed

$$\gamma_L(\cos \theta + 1) = 2(\gamma_S^{LW} \gamma_{L,i}^{LW})^{0.5} + 2(\gamma_S^+ \gamma_{L,i}^-)^{0.5} + 2(\gamma_S^- \gamma_{L,i}^+)^{0.5} \quad (\text{Eq. 1.13})$$

We used Eq. 1-13 with 3 different probe liquids to calculate SFEs of cathode materials for Li-ion batteries.[12]

1.3 Capillary Rising Method for Porous Materials

Contact angles of porous powders can be measured by capillary rising method. According to Washburn, we can calculate the contact angle of porous powder by measuring adsorbed liquid height by times.

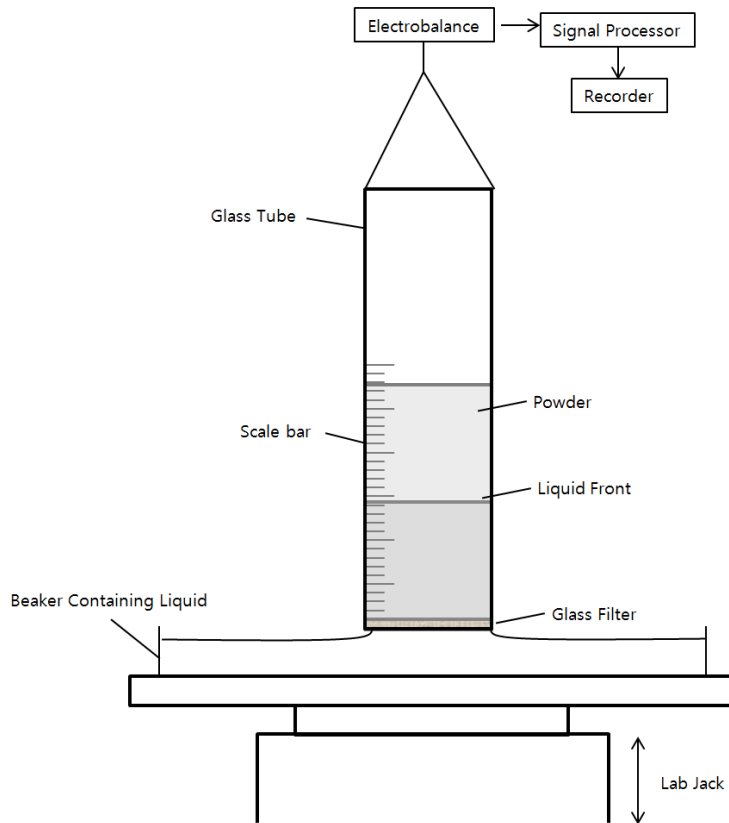


Fig. 2. Schematic experimental setup for contact angle measurements at powders[9]

Relations of capillary rising can be described by Washburn equation[13]

$$\frac{dh}{dt} = \frac{r^2}{8\eta h} \left(\frac{2\gamma_{lv}\cos\theta}{r} - \Delta\rho gh \right) \quad (\text{Eq. 1-14})$$

where h is the height of liquid penetration at time t , r is the radius of capillary. γ_{lv} is the liquid to vapor surface tension, θ is the contact angle, $\Delta\rho$ is the difference in density between the liquid and the gas phase, and η is the viscosity. Washburn equation can be measured by detection of m^2/t and can be simplified by measuring capillary constant. Capillary constant can be obtained by measuring m^2/t with totally wetting liquid (n-hexane).

$$\cos \theta = \frac{m^2}{t} \times \frac{\eta}{\rho^2 \sigma_L c} \quad (\text{Eq. 1-15})$$

$$c = \frac{1}{2} \pi^2 r^5 n_k^2 \quad (\text{Eq. 1-16})$$

where r is radius of the micro capillaries between powder particles, n_k is the number of powder particles. Capillary rising method cannot be used for above 90° : no liquid can penetrate to the powder above 90° [9, 13-15].

1.4 Dissolution Mechanism of Cathode Materials for Li-ion Batteries

Capacity fading of cathode materials for Li-ion batteries is highly dominated by decomposition product of LiPF_6 conducting salt and H_2O impurities in electrolyte.

Disproportionation (low potential)



Mn Dissolution by HF

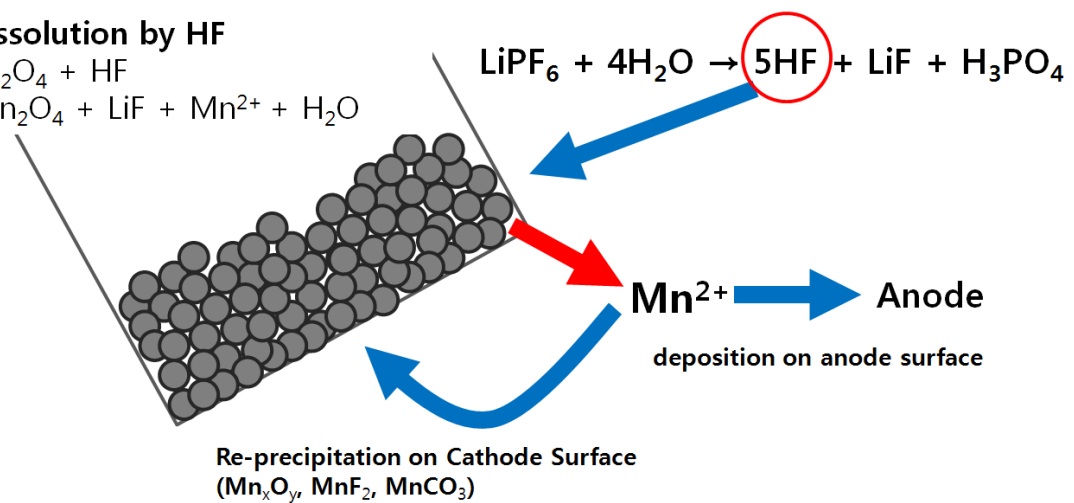
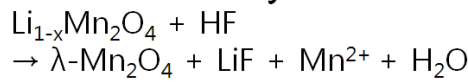


Fig. 3. Schematic description of dissolution mechanisms of LiMn_2O_4 [16]

Capacity is faded by the metal dissolution: it causes a loss of active material. In case of LiMn_2O_4 the MnF_2 , MnCO_3 and various oxides on the cathode has been observed increase in surface resistance. And also dissolved manganese can be incorporated in the solid electrolyte interface (SEI) of the carbon electrode. This phenomenon can induce the electrolyte decomposition and self-discharge of the lithiated carbon. Therefore, even a small amount of manganese in the electrolyte affect the cycle life of the Li-ion batteries[16].

1.5 Influence of Cathode Crystal Structure to Metal Dissolution

According to report of Hirayama, Ido, Kim, Cho, Tamura, Mizuki and Kanno [17], they confirmed the SEI layer structures on 111 and 110 plane surface of LiMn_2O_4 . SEI layer of 110 plane surface showed thicker and rougher surface than 111 plane. SEI layer prevent direct contact of electrode with electrolyte but it could not prevent Mn dissolution at 110 plane surface. But in 111 plane showed no significant deterioration. It means that the surface structure is important on the electrode stability.

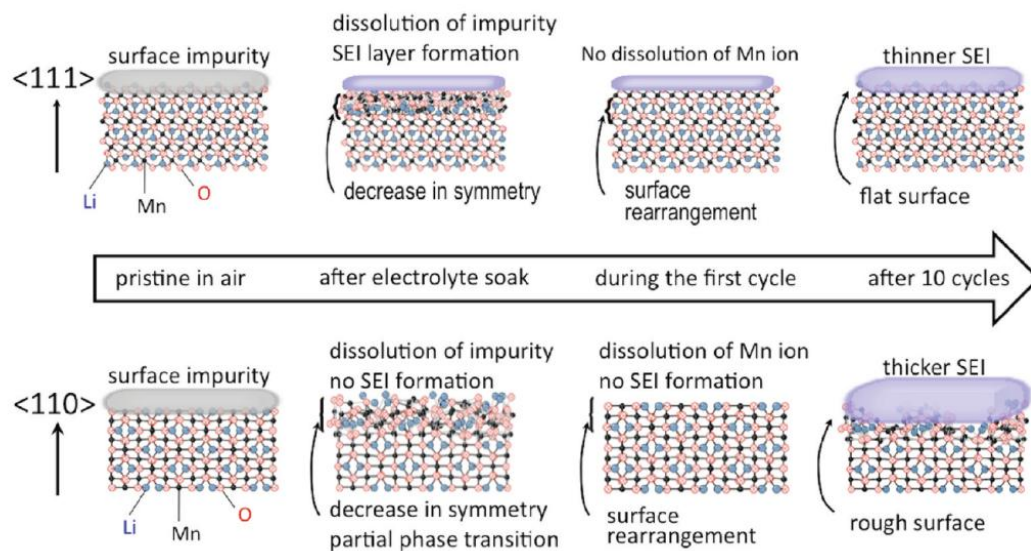


Fig. 4. Schematics of surface reactions for (111) and (110) crystal planes of LiMn_2O_4 characterized by in situ XRD and XRR measurements and ex situ TEM observations [17]

111 plane surface has higher surface energy than 110 plane surface, but after making SEI layer the thicker and rough surface on 110 plane has higher surface energy than thinner SEI layer on 111 plane. Therefore 111 plane is more stable in electrolyte than 110 plane [18-20].

1.6 Examples of Surface Free Energy Usages to analyze the characteristics of Li-ion Batteries

Surface polarity studies of alumina coated LiCoO₂ through measuring adsorbed SO₂ or NH₃ gaseous particles on the surface by XPS measurements were reported[21, 22].

sample	N/metal	S/metal
γ -Al ₂ O ₃	0.006	0.025
SnO ₂	0.051	0.023
TiO ₂ anatase	0.063	0.08
LiCoO ₂	0.06	0.75
LiCo _{0.75} Al _{0.25} O ₂	0.07	0.64
LiCo _{0.50} Al _{0.50} O ₂	0.06	0.36

Table 2. N/Metal and S/Metal ratios measured by XPS after adsorption of NH₃ or SO₂ at 80°C on LiCo_{1-x}Al_xO₂ Samples (0 ≤ x ≤ 0.50), compared with various oxides in the same experimental conditions [21]

Adsorbed SO₂ or NH₃ were decreased with increasing alumina ratio of cathode material:

Alumina lower the basicity of cathode material as it shown in table 1. But this method only predicts polarity of cathode material indirect way.

Surface polarity was also determined by using carbon dioxide adsorption microcalorimetry measurement: Carbon dioxide is acidic which expected to adsorbed more strongly on basic sites. CO₂ adsorption microcalorimetry measurements were carried out to determine the number, strength and strength distribution of the surface basic sites of the various cathode materials[23]. But it is also a indirect measurement.

2. Experimental

2.1 Sessil Drop Method

The Sessil drop method was used to measure contact angle of cathode electrodes for Li-ion batteries. DSA100 (Krüss, Hamburg, Germany) was used for contact angle measurement of cathode electrodes.

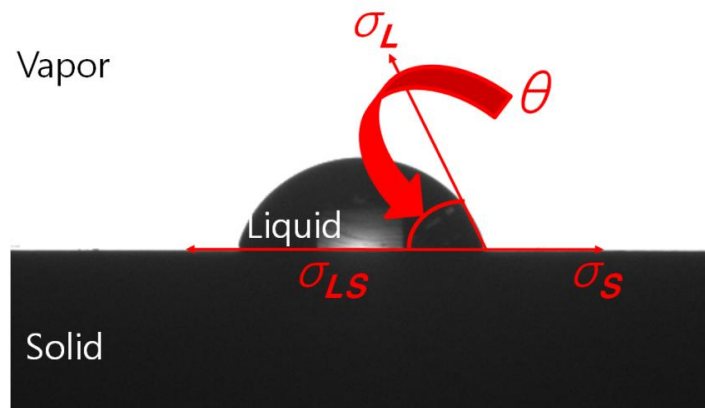


Fig. 5. Schematics of SFEs factors between solid, liquid and vapor

All cathode electrodes were stored in a 60°C vacuum furnace for over one day before measurement.

	γ_L	γ_L^d	γ_L^p	γ_L^+	γ_L^-
diiodomethane	50.8	50.8	0	0	0
formamide	58	39	19	2.28	39.6
water	72.8	21.8	51	25.5	25.5

Table 3. SFE properties of probe liquids [24]

Three probe liquids were used to measure the contact angle in order to calculate SFEs. Diiodomethane, formamide (Aldrich) and deionized water were used for probe liquids.

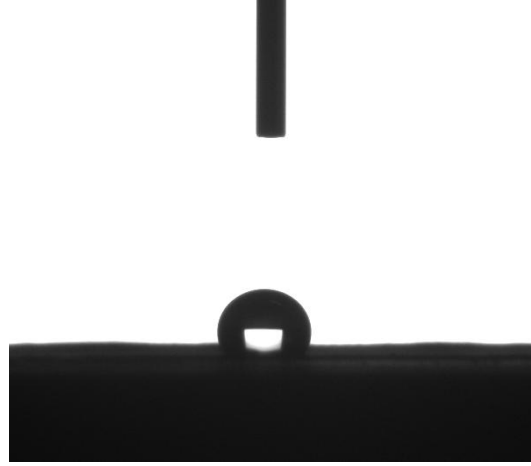


Fig. 6. Deionized water drop on LiCoO₂ Surface

The contact angles were measured as soon as the probe liquids dropped on the electrodes. Drop amount of probe liquids were kept same to compare each of materials in same condition. Young's equation[1] and van Oss-Chaudhury-Good (vOCG) equation[5] were used to calculate SFEs.

$$\gamma_S = \gamma_D + \gamma_L \times \cos\theta$$

Eq. 1. Young's equation[1]

$$0.5(1 + \cos\theta)\gamma_{L,i} = (\gamma_S^{LW} \gamma_{L,i}^{LW})^{0.5} + (\gamma_S^+ \gamma_{L,i}^-)^{0.5} + (\gamma_S^- \gamma_{L,i}^+)^{0.5}$$

(where, i=1, 2, 3)

$$\gamma_S = \gamma_S^D + 2(\gamma_S^- \gamma_S^+)$$

Eq. 2. van Oss-Chaudhury-Good (vOCG) equation[5]

2.2 Adsorption Method

The adsorption method (capillary rise technique) was used to measure the contact angles of the cathode powders for the Li-ion batteries. Tensiometer K100 (Krüss, Hamburg, Germany) was used for contact angle measurement of cathode powders filled in SH0620 fiber chambers as showed in the Fig. 6.



Fig. 7. Fiber chamber SH0620 (Krüss, Hamburg, Germany)

All powder samples were also stored in a 60°C vacuum furnace for over one day before measurement to dehydrate. The properties of the cathode powders were changed according to the time exposed to air due to the humidity. So the contact angles were measured within one hour. Capillary constant must be measured to determine the contact angles of porous materials such as cathode powder for Li-ion batteries. N-hexane was used to measure capillary constant which has only dispersity part, not any of polar part. So the capillary constant was calculated by using Washburn's equation due to the fact that the contact angle should be zero. So the $\cos\theta$ was equal to 1. The other terms are constant so, we can calculate the capillary constant.

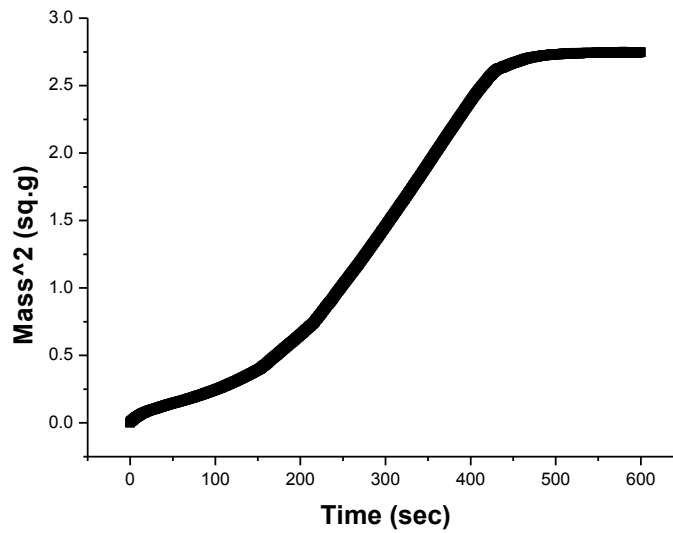


Fig. 8. Formamide adsorption mass change by time of LiCoO₂ powder

After that, by measuring mass changes by the adsorption of known probe liquids by time, the contact angles of powder cathode by each probe liquids were calculated by using Washburn equation (Eq. 3). The mass square changes by time were chosen of its maximum gradient after the filter noises. Fig. 4 shows mass changes by adsorbing probe liquid time of LiCoO₂ powder cathode.

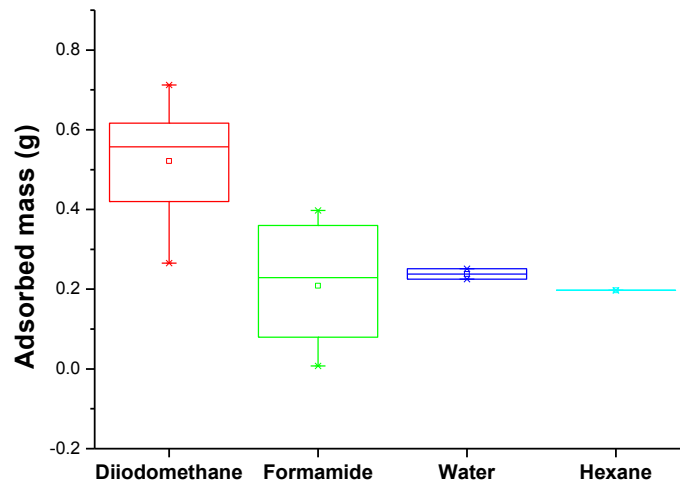


Fig. 9. Adsorped mass of probe liquids to filter

Fig. 5 shows the adsorped mass of probe liquids to filter. Diiodomethane adsorbed more and rapidly to the powder cathode than other probe liquids. So diiodomethane needed more cautious to loading the powder. To calculate SFEs of porous material the van Oss-Chaudhury-Good (vOCG) equation was used.

$$\cos \theta = \frac{m^2}{t} \times \frac{\eta}{\rho^2 \sigma_L c}$$

Eq. 3. Washburn's equation[13]

2.3 Measurement of Metal Dissolution

Metal dissolutions were measured by AAS to compare with SFEs. 1g of LiMn_2O_4 powders and a piece of electrodes for 2032 cell were stored in 60°C oven for 7days with 5ml of $\text{EC/EMC}=1/2$ LiPF_6 1mol electrolyte in teprone bottles. And LiCoO_2 powders and electrodes were stored in 60°C oven for 14days with 5ml $\text{EC/EMC}=1/1$ LiPF_6 1mol electrolyte in teprone bottles. All dissolution data were normalized by BET (specific surface area) to characterize the own surface characteristic not area effect of cathode materials.

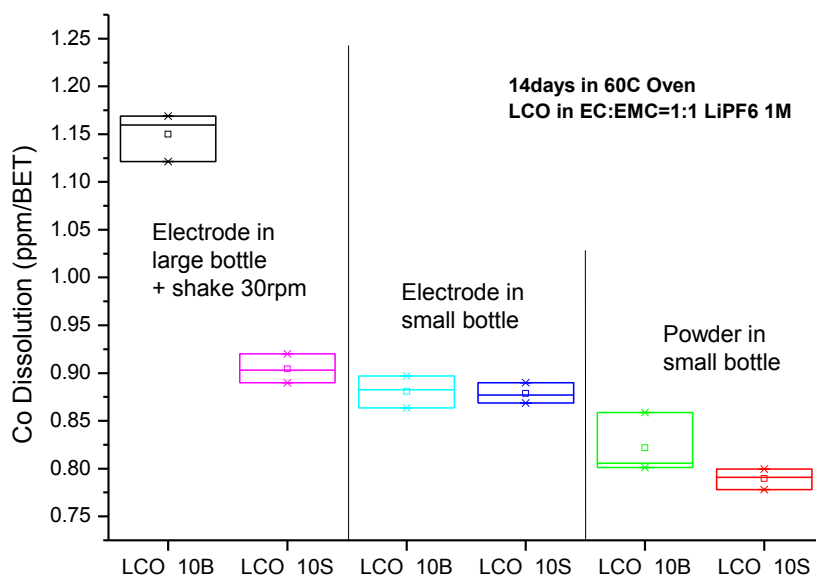


Fig. 10 Co Dissolution of LiCoO_2 with (a) Electrode in Large Bottle with Shaker (30rpm), (b) Electrode in Small bottle and (c) Same amount of powder of Electrode in Small Bottle

Various methods were tested, but the large bottle with shaker method was chosen due to it had more distinctness than other method as showed in Fig. 9.

3. Results and discussion

3.1 Correlation of the Surface Free Energies of LiMn_2O_4 Powder with Mn Dissolution

Various kind of LiMn_2O_4 powders were measured to correlate Mn dissolution with SFEs. Strong relationships between Mn dissolution and SFEs were confirmed by statistical analysis with Minitab software. By increasing total SFEs the Mn dissolution also increased.

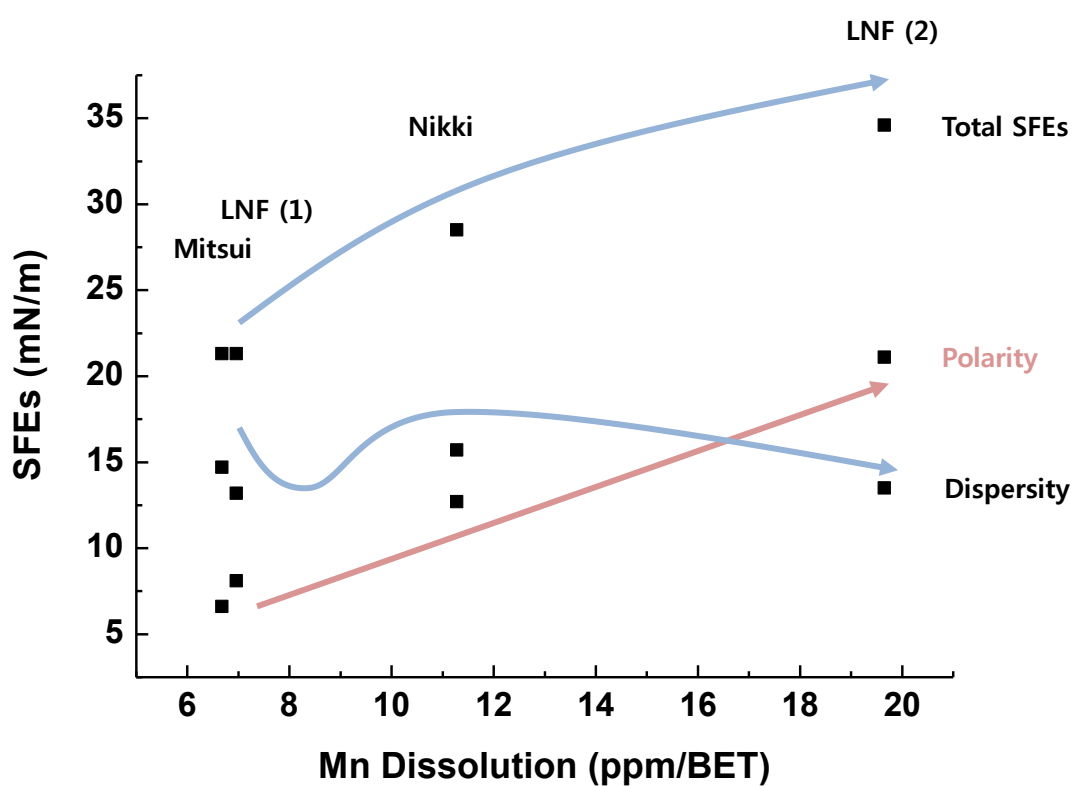


Fig. 11 Correlation of Mn dissolution with Total SFEs, polarity and dispersity of LiMn_2O_4 powder

Correlations: Dispersity, Polarity, SFE total, Mn Dissolution (ppm/BET)

	Dispersity	Polarity	SFE total
Polarity	-0.185		
	0.815		
SFE total	-0.002	0.983	
	0.998	0.017	
Mn Dissolution	-0.182	0.996	0.979
	0.818	0.004	0.021

Cell Contents: Pearson correlation

P-Value

Table 4. Correlations of surface free energies of LiMn₂O₄ powder with Mn dissolutions

Fig. 10 Show the correlations of Mn dissolution with SFEs. Statistical analysis was done to analyze the results quantitatively. Table 2 shows statistical analysis of correlations of Mn dissolution with SFEs. If the pearson correlation value closed to 1 which means it has higher correlation, and P-value under 0.05 has same meaning. The P-value of polarity with Mn dissolution was 0.004 that means it has very strong correlation. And total SFE with Mn dissolution showed 0.021 of P-value, but dispersity with Mn dissolution showed 0.818 of P-value which means it has no correlation. We confirmed very strong correlation between polarity and Mn dissolution.

3.2 Correlation of the Surface Free Energies of LiMn_2O_4 Electrode with Mn Dissolution

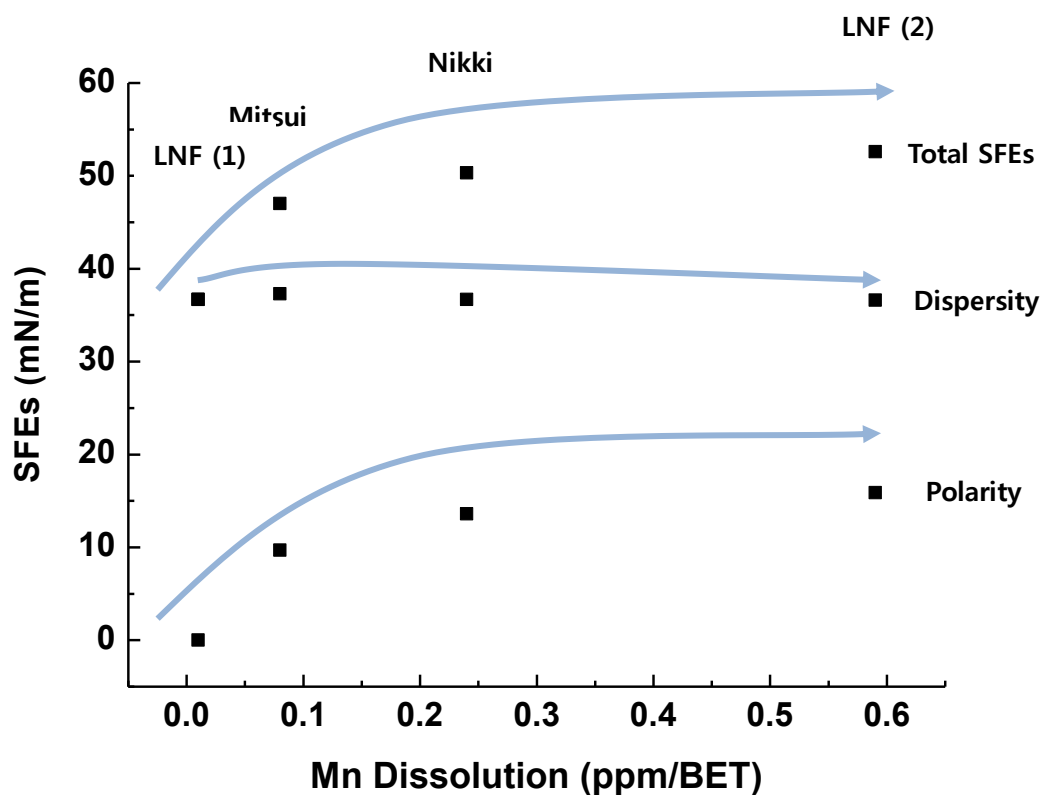


Fig. 12 Correlations of Mn dissolutions with (a) Total SFEs, (b) polarity and (c) dispersity of LiMn_2O_4 electrodes

Correlations of Mn dissolution of LiMn_2O_4 electrodes with SFEs were shown in Fig. 12. The correlations between SFEs and Mn dissolution of electrodes were weakened than the correlation of powder LiMn_2O_4 as shown Table.2 and 3: The LiMn_2O_4 electrodes were consist of cathode material, conductive carbon and binder. The conductive carbon and binder acted as noise due to the sessil drop method was used to measure the electrodes. And also those components made the SFEs of LiMn_2O_4 electrodes increased: Contact angles of LiMn_2O_4 electrodes were decreased by surface porosity.

Correlations: Dispersity, Polarity, SFE total, Mn Dissolution (ppm/BET)

	Dispersity	Polarity	SFE total
Polarity	-0.099		
	0.901		
SFE total	-0.057	0.999	
	0.943	0.001	
Mn Dissolution	-0.507	0.809	0.792
	0.493	0.191	0.208

Cell Contents: Pearson correlation

P-Value

Table 5. Correlations of surface free energies of LiMn₂O₄ electrodes with Mn dissolutions

3.3 Analysis the Crystal Structures of LiMn_2O_4

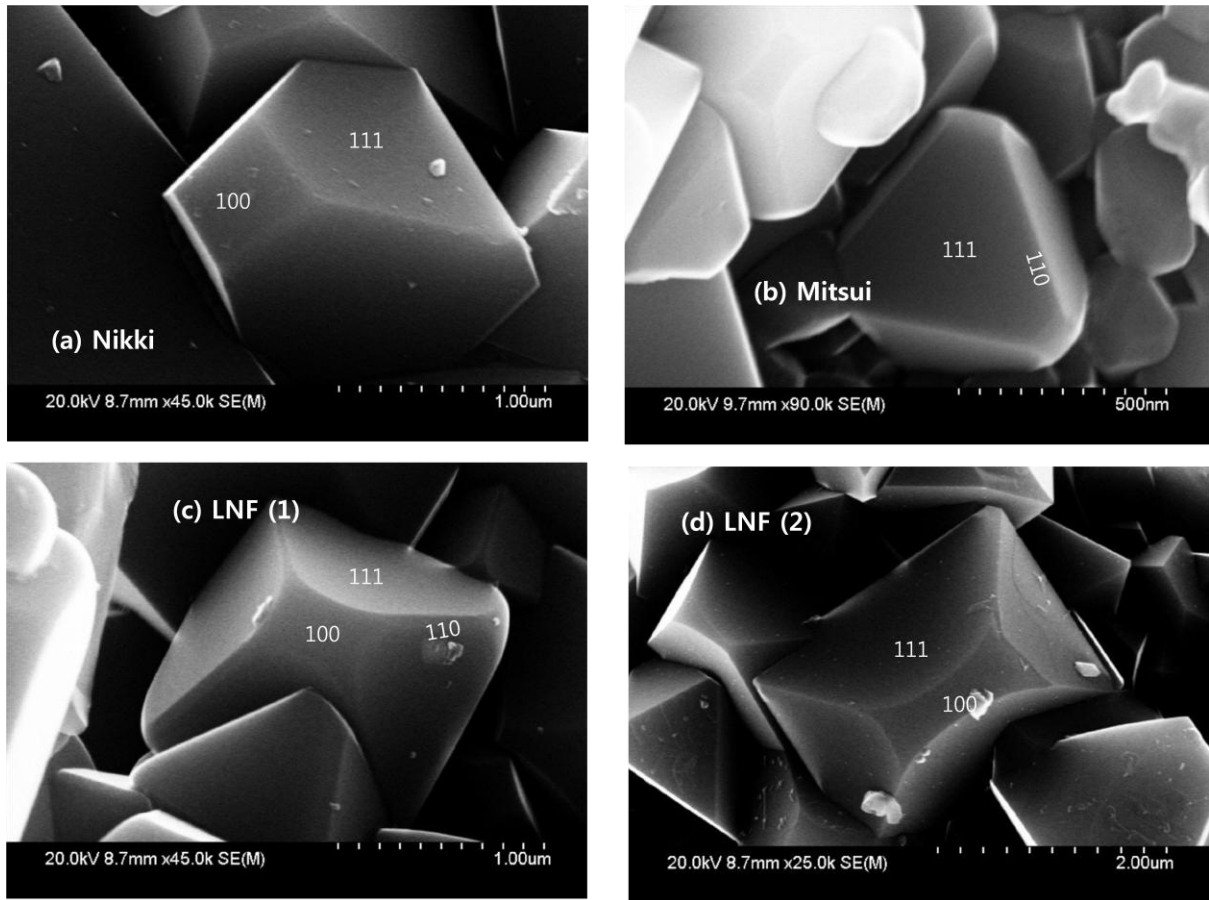


Fig. 13 SEM images of LiMn_2O_4 powders. (a) Nikki, (b) Mitsui, (c) LNF (1), and (d) LNF (2)

As we already know, optimized truncated octahedron structured LiMn_2O_4 shows better performance and lower Mn dissolution than pristine octahedral structure or not optimized truncated octahedral[25, 26]. All of the LiMn_2O_4 showed truncated octahedral structures, but Mitsui and LNF (1) showed smaller 001 plane surface than Nikki and LNF (2) and it showed 011 planes which were not showed in Nikki and LNF (2). So we can estimate that the optimized truncated octahedron structures should have 011 surface plane and proper portion of 001 surface plane. Optimized truncated octahedral showed less Mn dissolution and lower SFEs. So LiMn_2O_4 optimization can be done by measuring SFE.

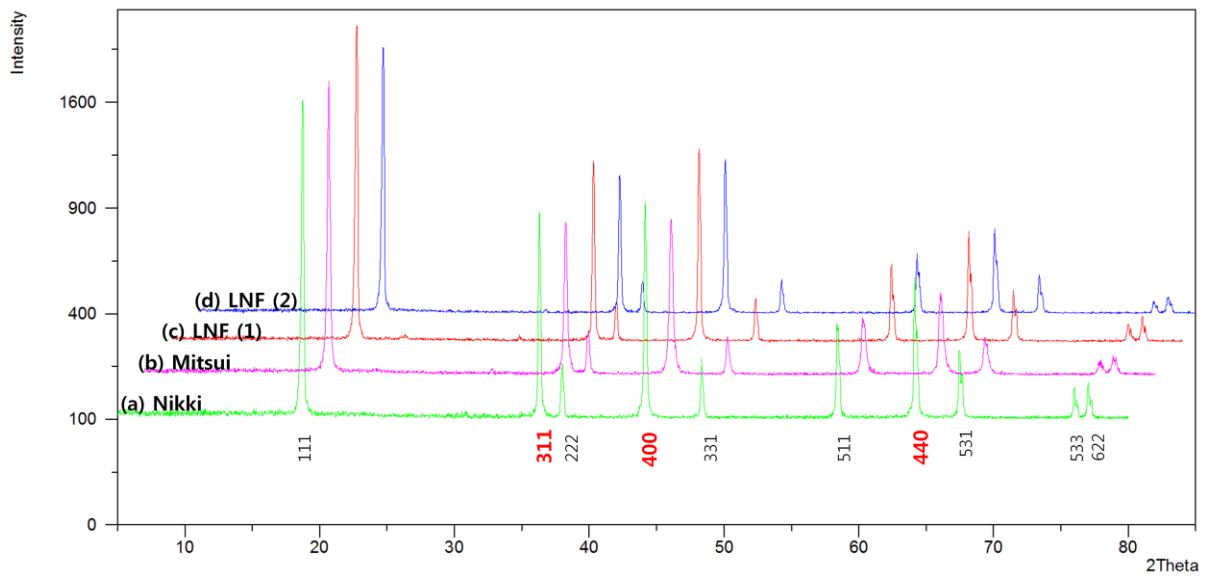


Fig. 14 XRD Patterns of LiMn_2O_4 powders (a) Nikki, (b) Mitsui, (c) LNF (1), and (d) LNF (2)

XRD patterns were also measured to confirm the crystal structure. Mitsui and LNF (1) showed broaden peaks in 311, 400 and 440 planes than Nikki and LNF (2). It showed that Mitsui and LNF (1) had more truncated octahedron structures than Nikki and LNF (2) [25].

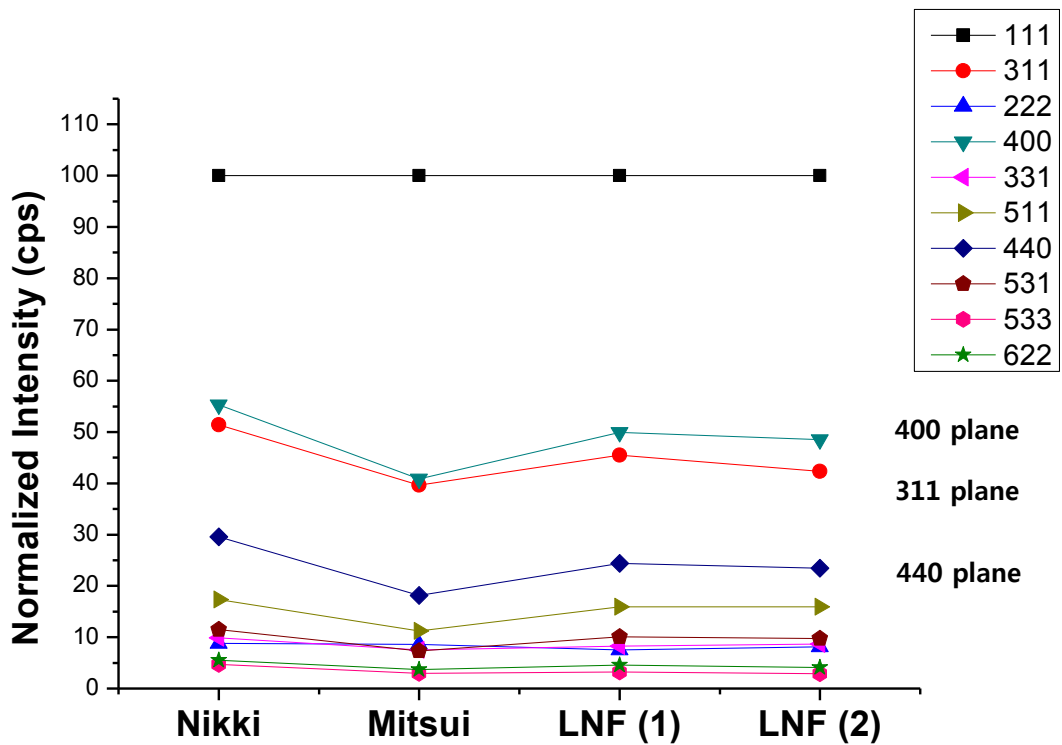


Fig. 15 Normalized XRD Peak by 100 Planes of LiMn_2O_4 Powders (a) Nikki, (b) Mitsui, (c) LNF (1), and (d) LNF (2)

Normalization of XRD peaks were done for comparison of plane compositions of each LiMn_2O_4 powders. Mitsui showed lowest peak intensities in 440, 311 and 440 planes which are known have higher SFE than other planes[25]. Mitsui showed lower portion of high SFE planes: Mitsui showed Lowest SFE and Lowest portion of 400, 311 and 440 planes. Portion of planes of Mitsui LiMn_2O_4 powder showed same result with SFE which means SFE can be used as an optimization criterion for crystal structures

3.4 Correlation of the Surface Free Energies of LiMn₂O₄ by increasing Al₂O₃ Coating amount with Mn dissolution

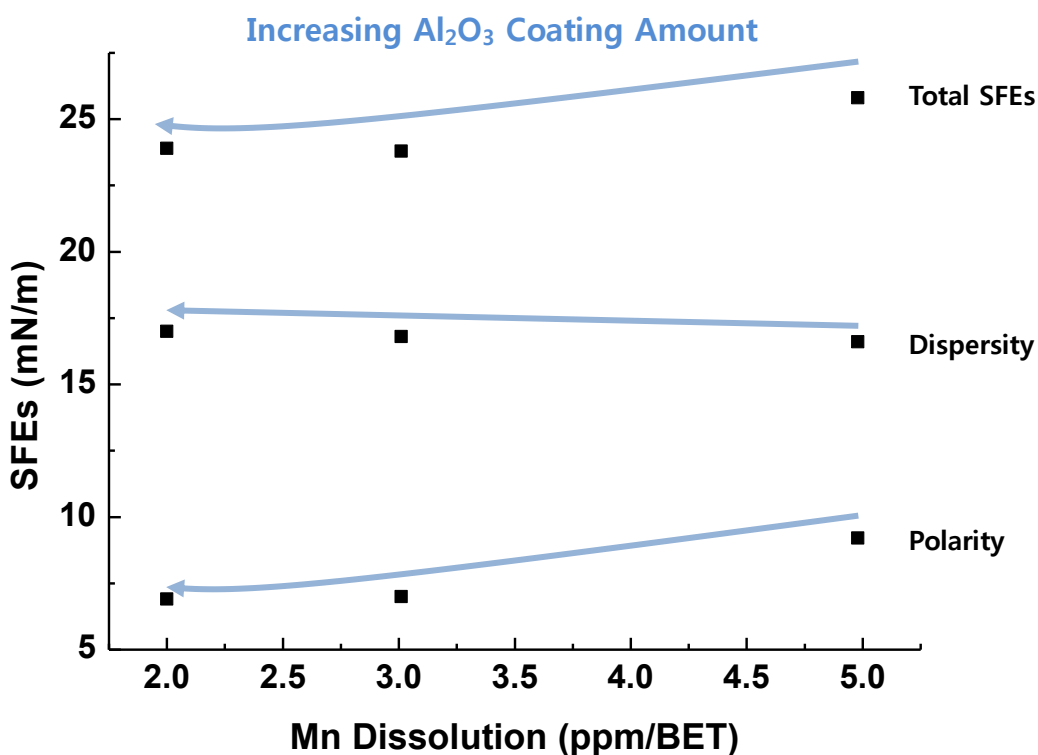


Fig. 14 Correlations of SFEs and Mn dissolution of LiMn₂O₄ powders by increasing Al₂O₃ coating amount with Total SFEs, polarity and dispersity

Correlations: Dispersity, Polarity, SFE total, Mn Dissolution (ppm/BET)

	Dispersity	Polarity	SFE total
Polarity	-0.885		
	0.309		
SFE total	-0.843	0.997	
	0.362	0.053	
Mn Dissolution	-0.983	0.955	0.927
	0.117	0.192	0.245

Cell Contents: Pearson correlation

P-Value

Table 6. Correlations of surface free energies of LiMn₂O₄ powder by increasing Al₂O₃ coating amount with Mn dissolutions

Al_2O_3 coating effects were tested with LiMn_2O_4 by increasing Al_2O_3 coating amount on the surfaces. By increasing Al_2O_3 coating amount the SFEs, Mn dissolution and cell capacity (data got from L&F Materials) were decreased. Polarity and SFEs total with Mn dissolution showed correlation of 0.192 and 0.245 of P-values, respectively. These values are not enough to determine which has strong correlation but, as it shown in Fig. 5 the Al_2O_3 coating was linearly affected the SFEs of LiMn_2O_4 . And also dispersity was increased with increasing amounts of Al_2O_3 coating which can be thought that dispersity of LiMn_2O_4 was changed (16.6 to 17mN/m) to the dispersity characteristic of Al_2O_3 (dispersity of Al_2O_3 : 23mN/m).

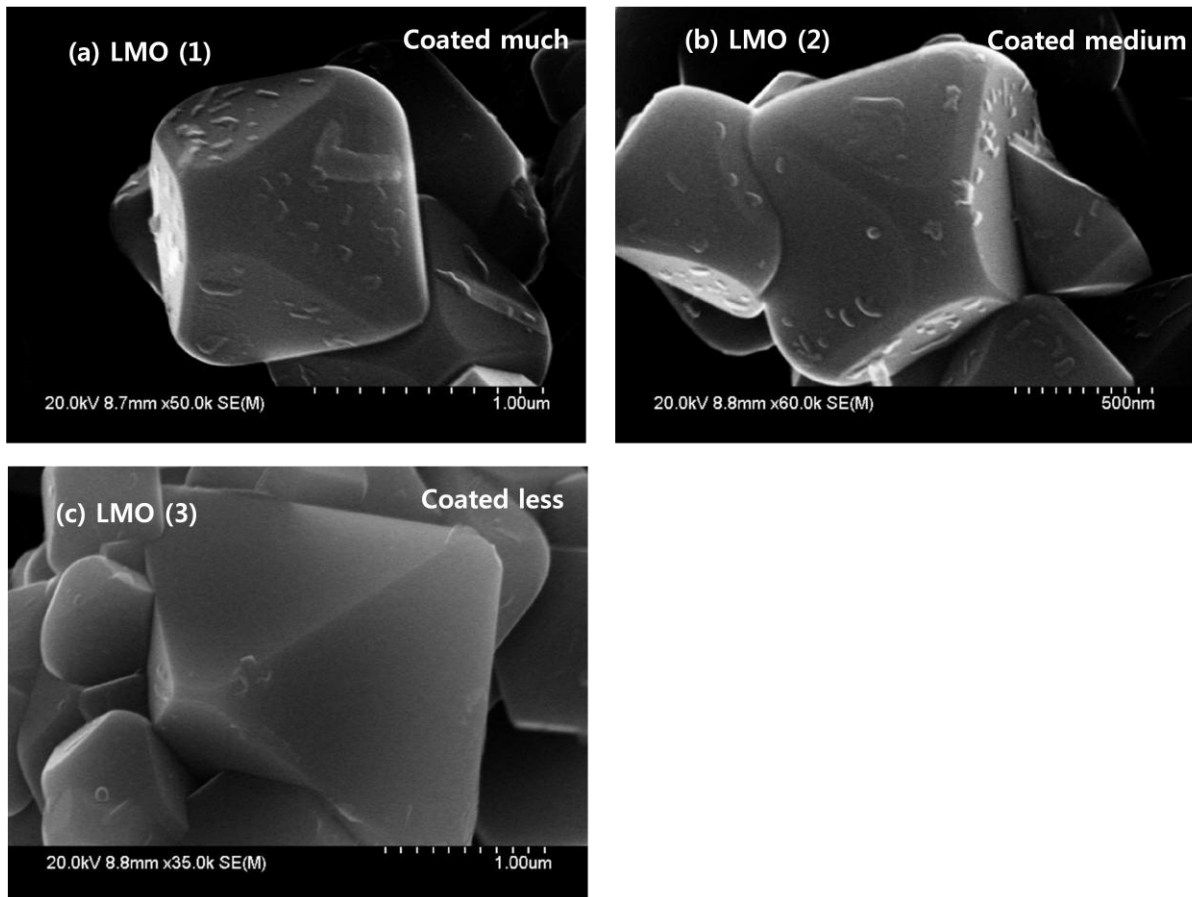


Fig. 15 SEM images of LiMn_2O_4 powders by increasing Al_2O_3 coating amount. Al was coated (a) much (b) medium (c) less on the LiMn_2O_4 surface

Surface of LiMn_2O_4 was well covered with Al_2O_3 by increasing Al_2O_3 coating amount as it shown in Fig. 15.

3.5 Acid and base part separation of Polar Surface Free Energy of LiMn_2O_4

Chemical reactions of Mn dissolution dominantly happen between F^- from Lithium Hexafluoro Phosphate (LiPF_6) salt in electrolyte and Mn^{2+} from Mn_2O_4 . Therefore the acid (electron acceptor: γ^+) part affects Mn dissolution of LiMn_2O_4 dominantly [16].

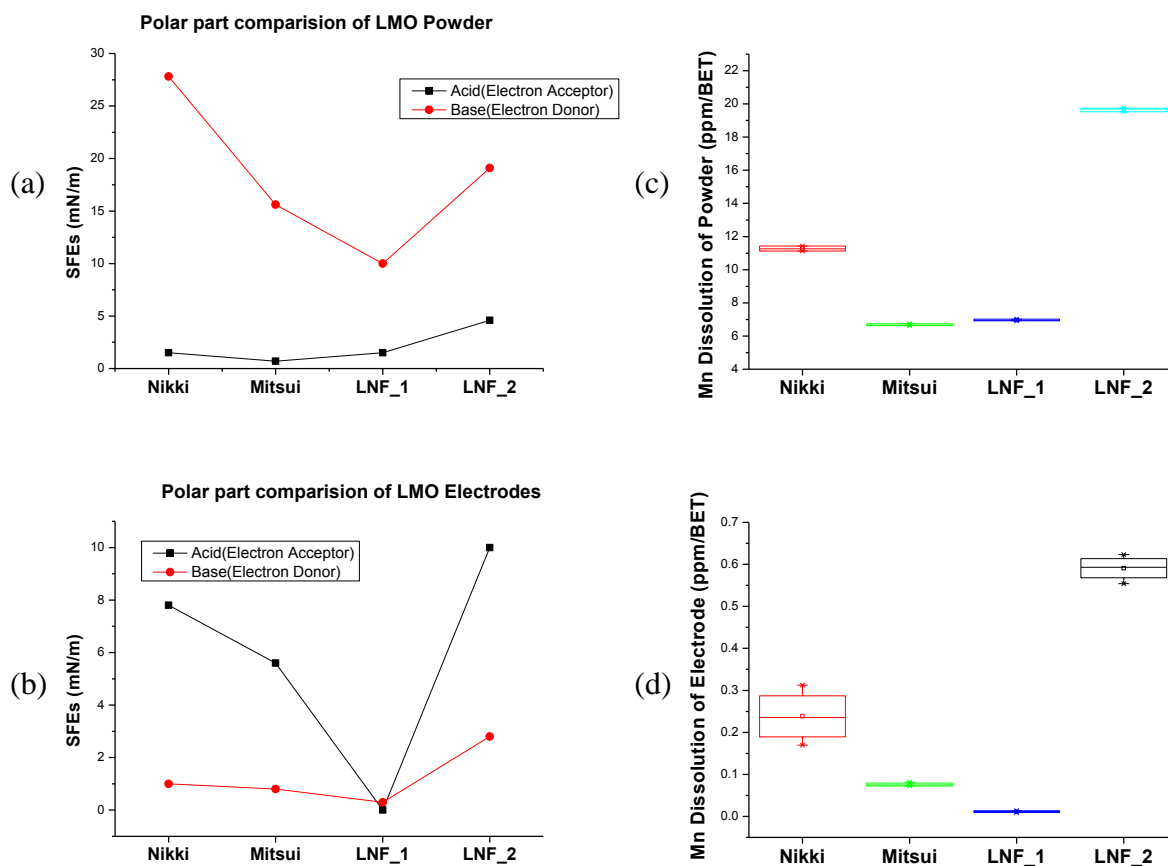


Fig. 16 Acid and base components of LiMn_2O_4 (a) powders and (b) electrodes and Mn dissolution of LiMn_2O_4 (c) powders and (d) electrodes

Fig. 16 showed the acid and base components of LiMn_2O_4 powders and electrodes. As shown in Fig. 16, base parts were dominant in polar parts in case of LiMn_2O_4 powders, but acid parts were dominantly affected the metal dissolution: Acid parts showed same trend with Mn dissolution as shown in Fig. 17. Acid parts were changed to main portion of total polar part and also showed same Mn dissolution trends with LiMn_2O_4 electrode. So the acid parts were dominantly affected Mn dissolution of LiMn_2O_4 .

3.6 Correlation of the Surface Free Energies of LiCoO₂ Powder with Co Dissolution

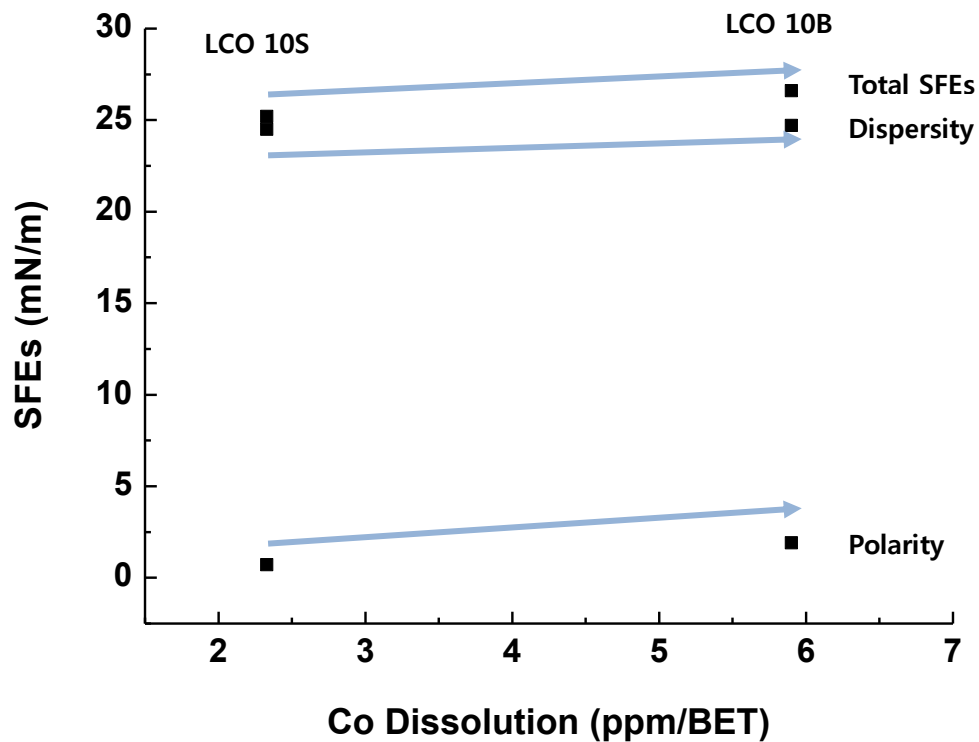


Fig. 18 Correlations of Co dissolutions with Total SFEs, polarity and dispersity of LiCoO₂ Powders

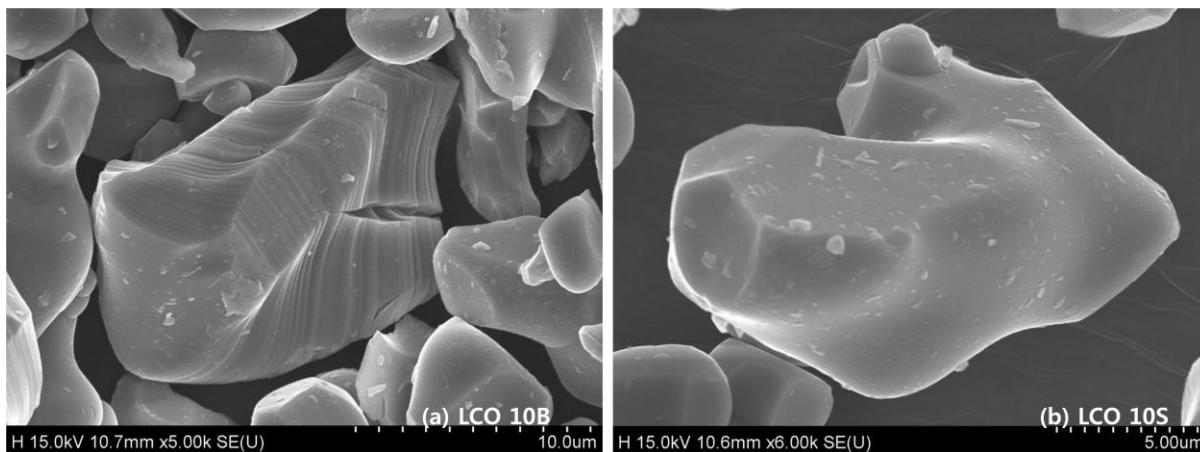


Fig. 19 SEM images of LiCoO₂ powders. (a) LCO 10B, (b) LCO 10S

As shown in Fig. 18, strong correlations between SFE of LiCoO_2 powders (of pristine: LCO 10B, Al_2O_3 coated: LCO 10S) and Co dissolution were confirmed. By increasing SFEs Co dissolution also increased. All components of SFEs of LiCoO_2 Powders were linearly fitted (which showed in Fig. 18) with Co dissolution not as LiMn_2O_4 cases showed in Fig. 13. Dispersities of LiCoO_2 were also changed (24.7 to 24.5mN/m) to the dispersity characteristic of Al_2O_3 (dispersity of Al_2O_3 : 23mN/m).

3.7 Correlation of the Surface Free Energies of LiCoO₂ Electrode with Co Dissolution

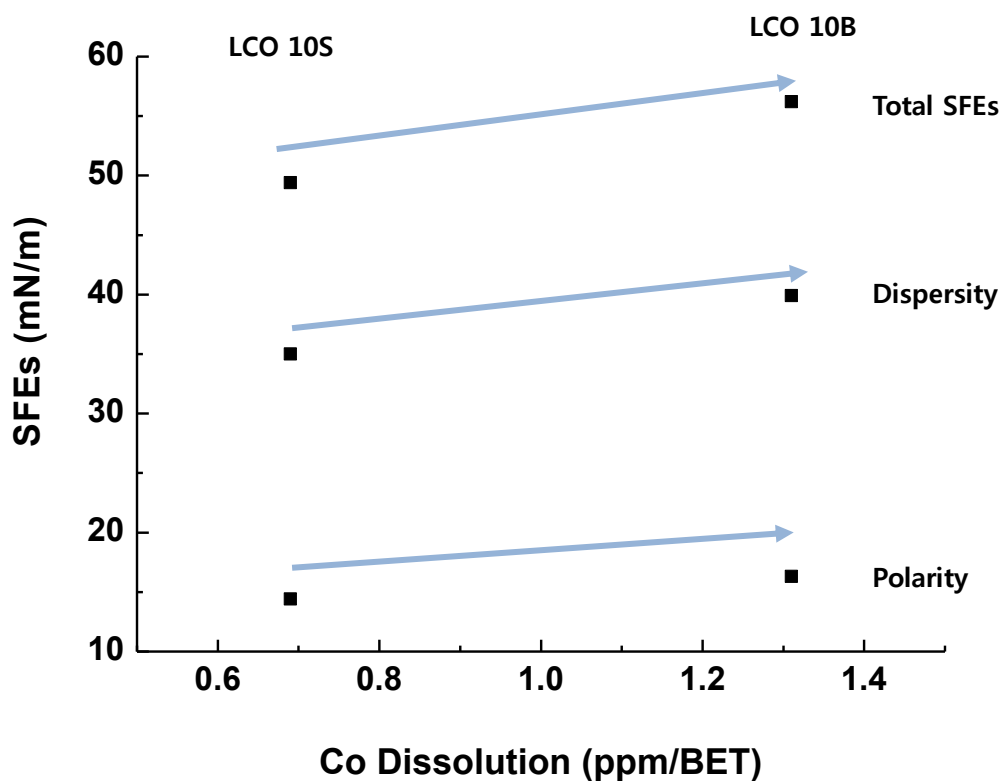


Fig. 19 Correlations of Co dissolutions with (a) Total SFEs, (b) polarity and (c) dispersity of LiCoO₂ Electrodes

Fig. 19 showed the correlation between SFEs of LiCoO₂ electrode and Co dissolution which were same as LiCoO₂ powders. But same as LiMn₂O₄ electrode, binders and conductive carbon made the SFEs of LiCoO₂ electrode increased: Contact angles of electrodes were decreased by porosity of surface.

3.8 Correlation of the Surface Free Energies of LiCoO₂ by increasing Al₂O₃ Coating amount with Co dissolution

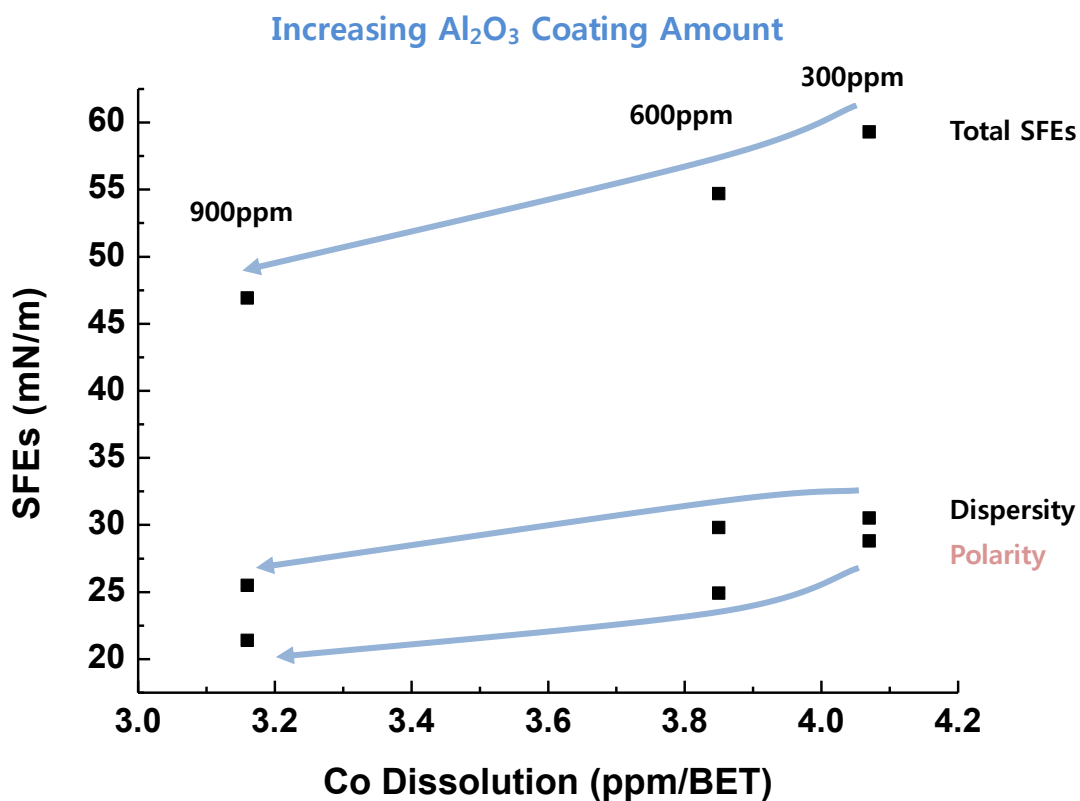


Fig. 20 Correlations of SFEs and Co dissolutions of LiCoO₂ powders by increasing Al₂O₃ coating amount with (a) Total SFEs (b) Polarity (c) Dispersity

Correlations: Dispersity, Polarity, SFE total, Co Dissolution (ppm/BET)

	Dispersity	Polarity	SFE total
Polarity	0.911		
	0.271		
SFE total	0.97	0.984	
	0.157	0.114	
Mn Dissolution	0.995	0.949	0.99
	0.066	0.204	0.09

Cell Contents: Pearson correlation
P-Value

Table 7. Correlations of surface free energies of LiCoO₂ powder by increasing Al₂O₃ coating amount with Co dissolutions

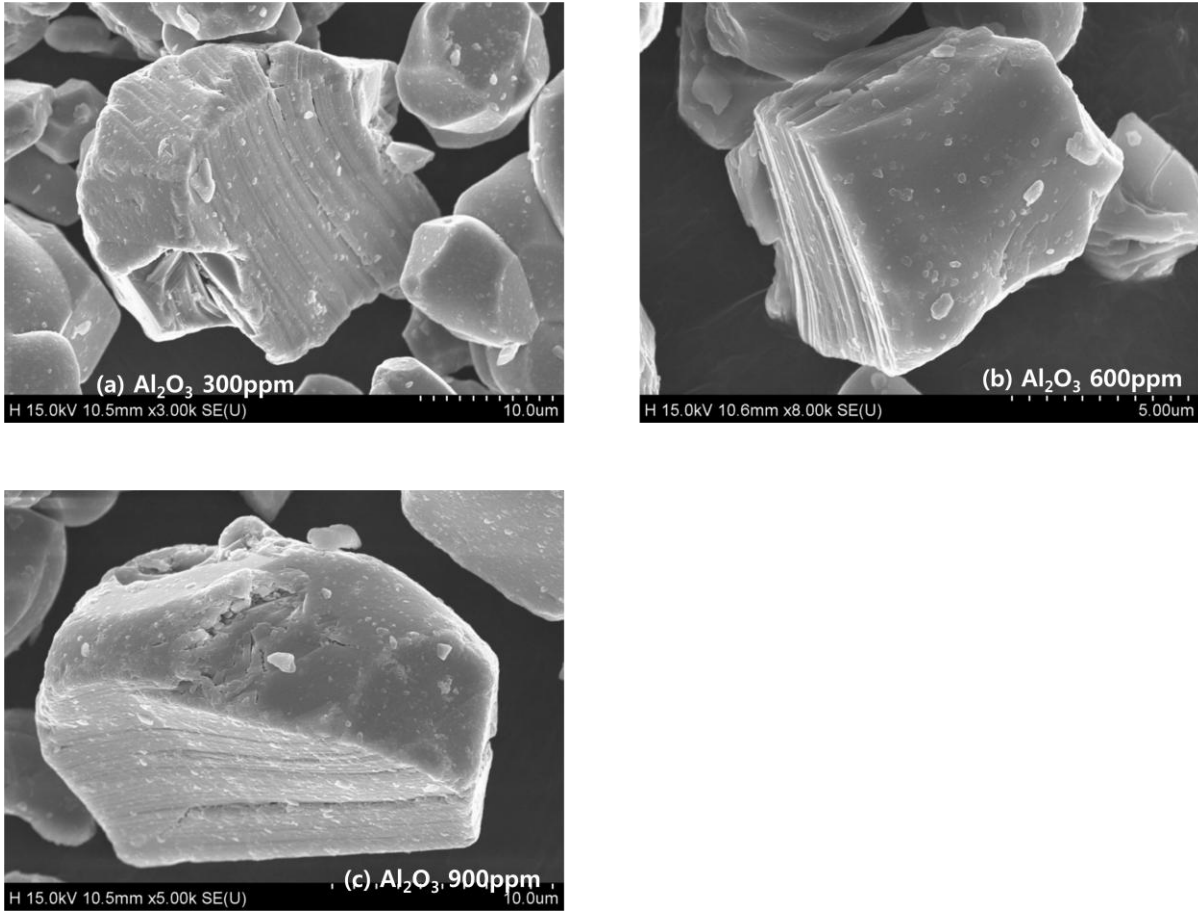


Fig. 22 SEM images of LiCoO₂ powders. (a) Al₂O₃ 300ppm, (b) Al₂O₃ 600ppm, and (c) Al₂O₃ 900ppm

All component of SFEs showed linear change by increasing Al₂O₃ coating amount which were shown in Fig. 20. The P-values were not under 0.05 but it showed 0.066, 0.204 and 0.09, respectively which were near 0.05 with Co dissolution can be thought as they have relationship. Dispersity of LiCoO₂ powder by increasing Al₂O₃ coating amount showed different trends(30.5 to 25.5mN/m) with LiMn₂O₄ cases, but the dispersities of LiCoO₂ were also changed to the dispersity characteristic of Al₂O₃ (dispersity of Al₂O₃: 23mN/m).

3.9 Acid and base part separation of Polar Surface Free Energy of LiCoO₂

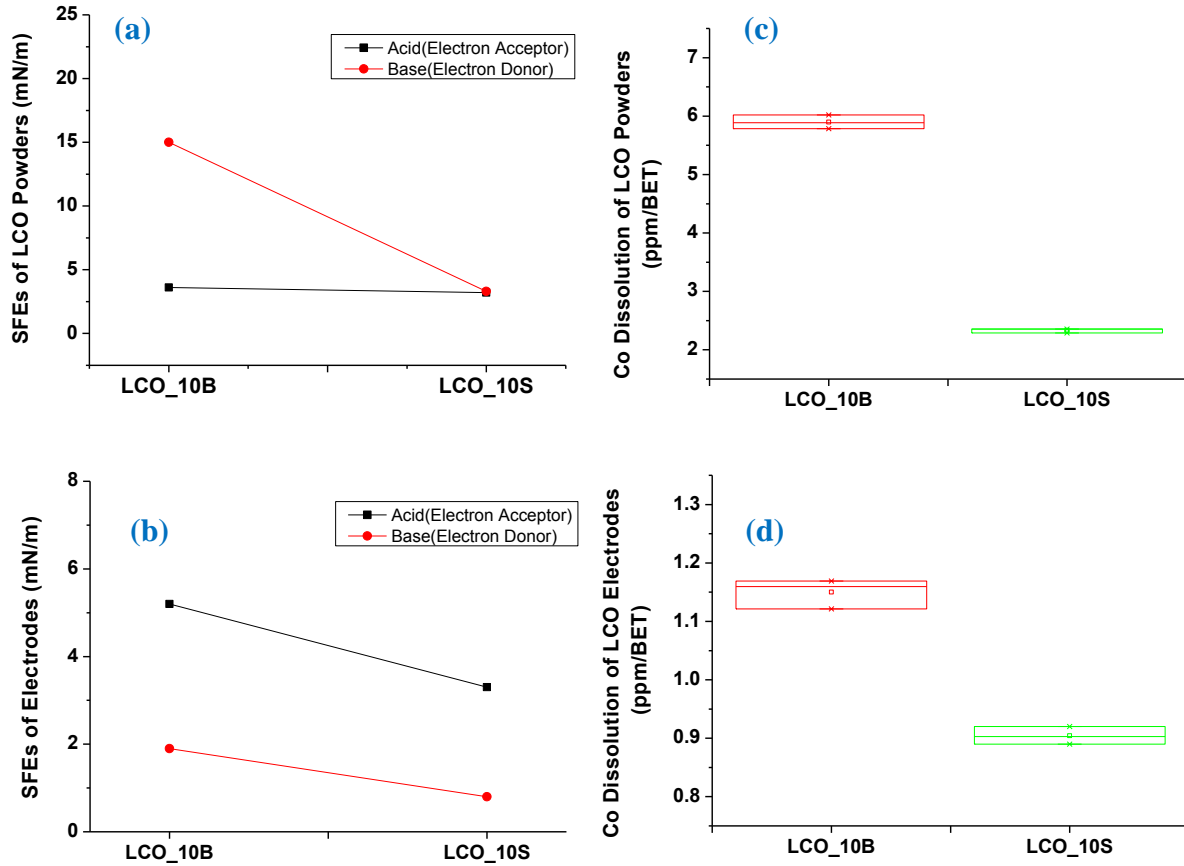


Fig. 21 Acid and base components of LiCoO₂ (a) powders and (b) electrodes and Co Dissolutions of LiCoO₂ (c) powders and (d) electrodes which were normalized by BET

Polar part separation of LiCoO₂ showed the same trends as LiMn₂O₄ cases as shown in Fig. 21. Base part was dominant in case of powder, but acid part changed to dominant portion of LiCoO₂ electrode. But the intensities changes of polar SFEs from powder to electrode between LiMn₂O₄ and LiCoO₂ showed different trend. It means LiMn₂O₄ and LiCoO₂ have different interaction mechanism with binder and conductive carbon. Therefore, to improve the characteristics of cathode materials, different binder or conductive carbon should be used for better optimization.

4. Conclusion

The SFEs of various kinds of LMO and LCO cathode materials for LIBs were evaluated in conjunction with their metal dissolution behavior. We confirmed the strong correlation between SFE and metal dissolution behavior of the cathode materials: The higher SFE, the higher metal dissolution. We also revealed that the polar component rather than the disperse one dominantly determine the metal dissolution of cathode materials. The impact of the polarity can be ascribed to the two factors: the acidic part of the polarity of cathode materials is related to the reactivity with F^- ions and the basic one to the reactivity toward H^+ ions in the electrolyte. The basic polar component of the electrode was much smaller than that of the powder. We also confirmed the correlation of the SFEs with the types of crystal structures, which were examined by using SEM and XRD analysis. Both commercialized and under developing $LiMn_2O_4$, showed truncated octahedral structures but the different ratios of the surface crystalline planes. With increasing 400 and 440 planes of $LiMn_2O_4$, the higher SFE and the metal dissolution was observed. This study suggests that the SFE characterization of the cathode materials can predict their metal dissolution behavior, and can be an optimization criterion of cathode crystal structure and surface coating materials.

References

- [1] T. Young, *Philos. Trans. R. Soc. London*, 95 (1805) 65-87.
- [2] D.K. Owens, R.C. Wendt, *J. Appl. Polym. Sci.*, 13 (1969) 1741-1747.
- [3] W.A. Zisman, *Ind. Eng. Chem.*, 55 (1963) 18-38.
- [4] F.M. Fowkes, *Ind. Eng. Chem.*, 56 (1964) 40-52.
- [5] C.J. van Oss, M.K. Chaudhury, R.J. Good, *Adv. Colloid Interface Sci.*, 28 (1987) 35-64.
- [6] B. Jańczuk, W. Wójcik, A. Zdziennicka, *J. Colloid Interface Sci.*, 157 (1993) 384-393.
- [7] F.M. Fowkes, *J. Adhes.*, 4 (1972) 155-159.
- [8] E. Chibowski, R. Perea-Carpio, *Adv. Colloid Interface Sci.*, 98 (2002) 245-264.
- [9] H. Dipl.-Phys. Hubert Lechner. Krüss, Germany, in, 1996.
- [10] C.J. Van Oss, R.J. Good, M.K. Chaudhury, *J. Colloid Interface Sci.*, 111 (1986) 378-390.
- [11] C.J. Van Oss, L. Ju, M.K. Chaudhury, R.J. Good, *J. Colloid Interface Sci.*, 128 (1989) 313-319.
- [12] M.-S. Wu, T.-L. Liao, Y.-Y. Wang, C.-C. Wan, *J. Appl. Electrochem.*, 34 (2004) 797-805.
- [13] E.W. Washburn, *Phys. Rev.*, 17 (1921) 273-283.
- [14] A. Lundblad, B. Bergman, *J. Electrochem. Soc.*, 144 (1997) 984-987.
- [15] C. Bakli, S. Chakraborty, *Appl. Phys. Lett.*, 101 (2012) 153112.
- [16] M. Wohlfahrt-Mehrens, C. Vogler, J. Garcke, *J. Power Sources*, 127 (2004) 58-64.
- [17] M. Hirayama, H. Ido, K. Kim, W. Cho, K. Tamura, J.i. Mizuki, R. Kanno, *J. Am. Chem. Soc.*, 132 (2010) 15268-15276.
- [18] K.K. Patel, J.M. Paulsen, J. Desilvestro, *J. Power Sources*, 122 (2003) 144-152.
- [19] J. Park, J.H. Seo, G. Plett, W. Lu, A.M. Sastry, *Electrochem. Solid-State Lett.*, 14 (2011) A14-A18.
- [20] R. Benedek, M.M. Thackeray, *Phys. Rev. B*, 83 (2011) 195439.
- [21] L. Dahéron, R. Dedryvère, H. Martinez, D. Flahaut, M. Ménétrier, C. Delmas, D. Gonbeau, *Chem. Mater.*, 21 (2009) 5607-5616.
- [22] N. Andreu, I. Baraille, H. Martinez, R. Dedryvère, M. Loudet, D. Gonbeau, *J. Phys. Chem. C*, 116 (2012) 20332-20341.
- [23] Y. Zhao, S. Wang, W. Ren, R. Wu, *J. Electrochem. Soc.*, 160 (2013) A82-A86.
- [24] C.S. Stefan, D. Lemordant, B. Claude-Montigny, D. Violleau, *J. Power Sources*, 189 (2009) 1174-1178.
- [25] J.-S. Kim, K. Kim, W. Cho, W.H. Shin, R. Kanno, J.W. Choi, *Nano Lett.*, 12 (2012) 6358-6365.
- [26] K.R. Chemelewski, D.W. Shin, W. Li, A. Manthiram, *J. Mater. Chem. A*, 1 (2013) 3347-3354.

국문요약

Li-ion 이차전지 양극재인 LiMn_2O_4 는 성공적으로 상업화되었고, EV 및 HEV 용 양극재 후보로서 각광을 받고 있으나 금속용출로 인한 비가역용량의 증가가 걸림돌이 되고 있다. 금속용출특성은 주로 ICP 혹은 AAS 를 이용하여 측정되고 있는데, 짧게는 일주일에서 길게는 수주까지 시간이 소요되었고 간접적인 양극재의 특성을 알 수 밖에 없었다.

본 연구에서는 측정시간이 수시간에서 수일 내이며 양극재의 직접적인 특성을 알 수 있는 표면자유에너지 분석을 통하여 용출특성을 예측하고자 실험을 진행하였으며, 표면자유에너지와 금속용출간의 강한 상관관계를 확인하였다. 전극은 Sessil drop 방식으로 파우더는 Adsorption 방식으로 접촉각을 측정하여 표면자유에너지를 계산하였는데, Polarity(Acidity, Basicity)가 Dispersity 에 비해 주도적으로 금속용출에 영향을 미치는 것을 확인할 수 있었다. Polarity 는 Al_2O_3 의 코팅량이 증가할수록 감소하는 것을 뚜렷이 확인할 수 있었으며, Dispersity 는 Al_2O_3 의 특성에 근접하는 것을 확인하였다. 파우더에서 전극으로 코팅되면서 Basicity 가 감소하는 것을 확인할 수 있었는데 코팅시 조건을 최적화하여 금속용출량을 감소시킬 수 있을 것으로 생각된다. 결정구조에 따른 표면자유에너지와 용출과의 상관관계도 분명히 확인할 수 있었다.

결론적으로 본 연구에서는 양극재의 표면자유에너지특성분석으로 용출특성 예측 및 표면(코팅, 결정구조) 변화에 따른 특성변화 분석이 가능하며, 특성최적화의 척도로서 이용될 수 있다는 사실을 확인하였다.

핵심어 : 금속용출, 표면자유에너지, 결정구조, 최적화, 극성

Acknowledgement (감사의 글)

학부를 졸업하고 회사에서 6년간 생활을 하다 보니 연구원으로서 한계가 느껴지기 시작하고 고향에 대한 향수가 커지던 차 고향인 대구에 있는 DGIST에서 석사과정을 모집한다는 소식을 친구 주희(남자)를 통해 듣게 되었습니다. 전액 장학금에 기숙사까지 제공하고 전세계의 석학들까지 모셔온다는 소식을 듣고 학교를 합격하기도 전인 4월에 고액연봉(?)을 받던 회사를 과감히 그만두고 가을학기 입학에 준비하였습니다. 입학하는데 도움을 준 주희(♂), 준형이형, 영준이 고맙습니다. 사실 처음에는 Solar Cell을 전공하고자 입학을 하였는데, 제가 하던 분야(무기)와는 다른 유기합성 Lab이어서 한 한기 동안 많이 방황을 하였습니다. 고심한 끝에 리튬이차전지 개발 랩인 ELSE랩으로 가기로 마음먹고 이호춘교수님을 찾아 뵈었는데 따뜻하게 받아주셔서 정말 감사했습니다. 무사히 석사과정을 마칠 수 있게 도와주셔서 감사합니다.

처음 ELSE랩에 들어와 많이 알려준 똥똥한 동휘, 먹보 은영이, 만형 성진이형 고맙습니다. 그리고 나에게 처음 표면자유에너지 실험주제를 토스한 승훈이 고맙다. 표면자유에너지에 관해 많이 알려주시고 실험방향에 대해 많은 조언 해 주신 L&F Material 최수안소장님 감사 드립니다. 실험 Sample 만들어준다고 고생한 화영이도 고맙다. 토하는 나를 이끌고 등산길에 동행해 준 성효, 그런 나에게 추월 당한 힙합브로 기성이 고맙다. 스타라이벌(?) 경구, 나에게 실험주제 토스 당한 성모, ELSE의 중심을 잡아주는 현진이도 고맙다. 힘들 때 마다 군말 없이 술친구 해준 영준이, 종완이, 대구에 있어서 한번씩 맛난 안주에 술 사준 세안이 고맙다. 회사에서 고생하며 번 돈 동생 살림살이에 다 퍼준 형님아 고맙다. 늦은 나이에 공부를 다시 한다고 했을 때 뜻대로 하게 해 주신 아버지 고맙습니다. 건강하게 오래오래 같이 사셨으면 좋겠네요. 사랑해요. 하늘에 계신 엄마도 제가 대기업에 입사하고, 석사도 하고, 결혼도 하는 모습을 보셨으면 정말 좋았을텐데..., 하늘에서 다 지켜보고 계시죠? 덕분에 무사히 석사도 졸업했어요 ^^ 사랑해요. 그리고 결혼을 허락 해 주신 장인어른, 따뜻하게 저를 맞아주신 장모님, 처제 학연이, 처남 학민이 고맙습니다. 할머니의 병간호와 아버지 옆에서 엄마의 빈자리를 채워주신 분께도 감사 드립니다.

마지막으로 학생인 나를 믿고 시집와주고 예쁜 딸 예지까지 얻게 해준 학용이에게 너무 고맙고 많이 사랑한다♥

Curriculum Vitae

Name: Junmin Lee

Birth Date: 1981.02.16

Education

1999-2006 B.S., Physics, Yeungnam University

2011-2013 M.S., Department of Energy Systems Engineering, DGIST

Work Experience

2006-2011 Research Engineer, OLED Development Department, LG Display

Honors and Award

2009. 12. CEO Silver Award of TDR